Generation of the Southern Ocean pycnocline by sea ice-ocean interactions

A. Klocker[1,2*], A. C. Naveira Garabato[3], F. Roquet[4], C. de Lavergne[5], S. R. Rintoul[6,7,8]

[1]Institute for Marine and Antarctic Studies, University of Tasmania, Hobart, Australia
[2]Australian Research Council Centre of Excellence for Climate Extremes, University of Tasmania, Hobart, Australia
[3]Ocean and Earth Science, National Oceanography Centre, University of Southampton, Southampton, United Kingdom
[4]Department of Marine Sciences, University of Gothenburg, Gothenburg, Sweden
[5]LOCEAN Laboratory, Sorbonne University-CNRS-IRD-MNHN, Paris, France
[6]Commonwealth Scientific and Industrial Research Organisation, Oceans and Atmosphere, Hobart, Australia
[7]Centre for Southern Hemisphere Oceans Research, CSIRO, Hobart, Australia
[8]Australian Antarctic Program Partnership, University of Tasmania, Hobart, Australia

Key Points:

- The Southern Ocean's permanent pycnocline is generated by seasonal sea ice-ocean interactions.
- Sea-ice melt leads to the formation of a salinity-based stratification at the base of the winter mixed layer.
- The permanent pycnocline descends into the ocean interior at fronts of the Antarctic Circumpolar Current.

*Department of Geosciences, University of Oslo, Oslo, Norway

Corresponding author: Andreas Klocker, andreas.klocker@geo.uio.no

Abstract

The ocean's permanent pycnocline is a layer of elevated stratification that separates the well-ventilated upper ocean from the more slowly-renewed deep ocean. Despite its pivotal role in organizing ocean circulation, the processes governing the formation of the permanent pycnocline remain little understood. Two factors in particular are generally overlooked: the presence of a zonal channel in the Southern Ocean, and the nonlinear interplay between temperature and salinity distributions. Here we assess the mechanism generating the Southern Ocean's permanent pycnocline through the analysis of a high-resolution, realistic, global sea ice-ocean model. We show that the permanent pycnocline is formed by seasonal sea ice-ocean interactions in two distinct ice-covered regions, fringing the Antarctic continental slope and the winter sea ice edge. In both areas, persistent sea ice melt leads to the formation of strong, salinity-based stratification at the base of the surface mixed layer in winter. The resulting sheets of high stratification subsequently descend into the ocean interior at fronts of the Antarctic Circumpolar Current, and are projected equatorward into the Southern Hemisphere basins along density surfaces. Our findings thus highlight the crucial role of localized sea ice-ocean interactions in configuring the vertical structure of the Southern Ocean.

Plain Language Summary

Satellite observations have revealed significant trends in sea ice concentration over recent decades. While the science community is starting to unravel the causes of the observed changes in sea ice extent, our understanding of how these ice changes are influencing ocean circulation remains rudimentary. Here we take a step toward addressing this critical gap by showing – through the analysis of a state-of-the-art, realistic sea ice-ocean model – that localized sea ice-ocean interactions in the Southern Ocean, in particular the melting of sea ice, configure the vertical structure of the Southern Hemisphere oceans.

1 Introduction

The permanent pycnocline (not to be confused with the *ventilated pycnocline* (Luyten et al., 1983), which refers to the shallower, relatively weakly stratified and well-ventilated portion of the pycnocline at the base of subtropical gyres) is a perennial layer of elevated density stratification, found at 200-1500 m over much of the ocean (Samelson & Vallis,

1997; Gnanadesikan, 1999). It is the main organizing feature of global ocean circulation, as it separates the relatively well-ventilated waters of the upper ocean, including those of the ventilated pycnocline, from more slowly-renewed deeper waters (DeVries & Primeau, 2011). The abrupt vertical gradient in renewal time scale associated with the permanent pycnocline structures many important oceanic physical and chemical properties, such as salinity (Fig. 1 b,d,f) or dissolved inorganic carbon (DeVries & Weber, 2017), thus fundamentally shaping the ocean's climatic role.

Classical views of the pycnocline – historically referred to as thermocline theory, since past work has focused on regions where stratification is set by temperature (often termed the *alpha ocean*, see (Carmack, 2007)) – propose two distinct mechanisms of pycnocline formation. In adiabatic theories (Welander, 1959; Luyten et al., 1983; Huang, 1988), the surface density distribution is set by atmospheric thermal forcing and transferred to the ocean interior by wind-driven Ekman downwelling, which maps the surface meridional density gradient to a vertical profile. In contrast, diabatic theories (Robinson & Stommel, 1959; Stommel & Webster, 1962; Young & Ierley, 1986; Salmon, 1990) interpret the pycnocline as a diffusive front (or internal boundary layer) that forms at the convergence of warm near-surface waters and upwelling cold abyssal waters. In this view, the pycnocline thickness decreases as diabatic mixing weakens. Such adiabatic and diabatic perspectives on pycnocline generation were subsequently unified in a two-regime model (Samelson & Vallis, 1997), according to which an upper, adiabatic part of the pycnocline (the ventilated pycnocline) results from the vertical mapping of the surface meridional temperature gradient across the subtropical gyre; and a lower, diabatic part of the pycnocline (the internal, or permanent, pycnocline) is generated via a vertical advection - diffusion balance, which recasts the surface meridional temperature difference across the subpolar gyre onto the vertical. This two-regime model, derived for a single-hemisphere closed basin, reproduces the main characteristics of the subtropical pycnocline and constitutes, to this day, the standard point of reference upon which our understanding of the pycnocline is based.

However, classical pycnocline theories do not directly address where or how extensive parts of the permanent pycnocline, in particular that pervading in the Southern Ocean, are formed. To elucidate this question, at least two limitations of classical pycnocline theories must be considered. First, these theories overlook the impact of the Southern Ocean's zonal channel, thought to lead to a markedly different pycnocline structure as well as the

emergence of a vigorous inter-hemispheric overturning circulation (Vallis, 2000; Nikurashin & Vallis, 2012). Although more recent renditions of pycnocline theory have identified a focal generative role for the Southern Ocean, they either assume the existence of (Gnanadesikan, 1999), or fail to reproduce (Wolfe & Cessi, 2010; Nikurashin & Vallis, 2012), the mid-depth stratification maximum that defines the permanent pycnocline.

Second, classical pycnocline theories assume, through their focus on temperature stratification, a minor role for salinity. As they effectively treat density as a conservative quantity, the theories disregard potentially influential nonlinear interactions between the distributions of temperature and salinity. These nonlinear interactions may arise in two main ways: (i) via density's nonlinear dependence on temperature, salinity and pressure; and (ii) via the forcing of surface heat and freshwater fluxes through distinct mechanisms with different spatio-temporal scales. Nowhere is the significance of such nonlinear interactions more evident than in polar regions. There, the dominance of salinity in determining upper-ocean stratification (in the so-called *beta ocean*) maintains vast volumes of warm waters below the pycnocline and favours the wintertime formation of sea ice (Carmack, 2007) – the presence of which creates a powerful coupling between heat and freshwater fluxes (Martinson, 1990; Polyakov et al., 2017; Lecomte et al., 2017; Wilson et al., 2019). Recent work demonstrates the prominent global stratification impact of the nonlinear dependence of density on temperature and pressure (Nycander et al., 2015; Roquet et al., 2015), and highlights the large sensitivity of global stratification to seawater properties near the freezing point (Roquet et al., 2015).

In this paper, we show that the two key elements missing from the classical pycnocline paradigm (specifically, Southern Ocean geometry and nonlinear interactions between temperature and salinity patterns) play an important role in the generation of the permanent pycnocline of the Southern Hemisphere oceans. Our illustration of this result is framed in terms of potential vorticity (PV). Although vigorously modified at the ocean surface, PV is approximately conserved in the ocean interior, where diabatic and frictional processes are generally weak (Luyten et al., 1983). Here we define $\mathrm{PV} = -\frac{f}{\rho}\frac{d\rho}{dz}$, where f is the Coriolis parameter, ρ is the surface-referenced potential density, and $\frac{1}{\rho}\frac{d\rho}{dz}$ quantifies the vertical stretching of isopycnal layers. Relative vorticity is neglected in this definition, as it is small relative to planetary vorticity except in localized frontal regions (J. Marshall et al., 1993). Thus, PV is closely related to stratification, and the pycnocline—a comparatively thin layer of high stratification—is found to comprise several two-dimensional

surfaces along which PV is elevated. We will refer to these two-dimensional surfaces as *high-PV sheets*.

2 Data and Methods

2.1 Model description

Observations of seasonal surface forcing in conjunction with subsurface hydrography in the Southern Ocean are presently scarce. We therefore turn to an eddying global sea ice-ocean simulation that has been thoroughly validated with observations and proven to be reasonably realistic (Kiss et al., 2020). The use of model output allows seasonally-varying surface fluxes to be linked to the seasonal evolution of stratification and PV. This enables us, in turn, to build an integrated picture of processes leading to the structure of the permanent pycnocline.

The simulation at the core of our analysis uses a mesoscale eddy-rich version of the sea ice-ocean implementation of the Australian Community Climate and Earth System Simulator, ACCESS-OM2, run at a horizontal resolution of 0.1^o (ACCESS-OM2-01) with 75 vertical levels. The ocean model is MOM5.1 and the sea ice model CICE5.1, coupled with the OASIS-MCT coupler. The model was forced with the JRA55-do v1.3 forcing data set. The ACCESS-OM2-01 experiment ran for 33 years from 1 January 1985 to 31 December 2017. It was started from a 40-year spin-up under repeated 1 May 1984 – 30 April 1985 JRA55-do forcing. Note that, while below we define the Stratification Control Index in terms of conservative temperature Θ and absolute salinity S_A, the model uses potential temperature θ and practical salinity S_P instead. Hence, both PV and the SCI in the model are calculated using θ and S_P. Details of the simulation and its evaluation can be found elsewhere (Kiss et al., 2020).

3 Results and Discussion

3.1 Relating potential vorticity to the Southern Hemisphere's ocean structure

The distribution of PV provides the organizing framework for the large-scale water mass structure and vertical circulation of the ocean. In the Southern Ocean and neighbouring Southern Hemisphere basins, this may be readily illustrated with meridional sections of PV across the Indian, Pacific and Atlantic sectors (Fig. 1). PV exhibits a lay-

ered arrangement, whereby thick layers of low PV are separated by thinner sheets of high PV. The thick, low-PV layers correspond to the major oceanic water masses, which feature prominently in syntheses of the Southern Hemisphere ocean circulation (Talley, 2013; A. C. Naveira Garabato et al., 2014).

Specifically, the low-PV layers extending northward from the Southern Ocean in both the Indian and Pacific basins at depths of < 800 m contain Subantarctic Mode Water (SAMW; Fig. 1 a-d). In the Atlantic basin, a low-PV layer residing at depths of $<$ 500 m encompasses Subtropical Mode Water (STMW; Fig. 1 e-f). The low-PV layers extending northward from the Southern Ocean in the Indian and Pacific basins (Atlantic basin) at depths of ~ 1000 m (~ 700 m) contain Antarctic Intermediate Water (AAIW). AAIW exhibits a broad sub-surface salinity minimum (Fig. 1 b,d,f). Both STMW / SAMW and AAIW are characterized by relatively short ventilation time scales (McCartney, 1977; DeVries & Primeau, 2011). The deepest low-PV layer visible in Figure 1 encompasses Circumpolar Deep Water (CDW), a voluminous, slowly-renewed water mass that has primordial sources in the North Atlantic and ultimately upwells in the Southern Ocean (Tamsitt et al., 2017). All of these water masses acquire their low PV at their surface formation sites, where intense wind and buoyancy forcings in winter trigger convective mixing and destroy stratification (Speer & Forget, 2001; Bullister et al., 2001).

In turn, the high-PV sheets bounding the low-PV layers define the fabric of the ocean's pycnocline. The high-PV sheet closely following the 27.15 kg m^{-3} (27.05 kg m^{-3}) isopycnal in the Pacific (Indian) basin embodies the SAMW-AAIW interface. A less pronounced high-PV sheet is found at higher density, following the 27.5 kg m^{-3} (27.45 kg m^{-3}) isopycnal in the Pacific (Indian) Ocean, and constitutes the AAIW-CDW interface. A similar framework of two high-PV sheets exists in the Atlantic basin, where the sheets follow lighter isopycnals than in the Indo-Pacific sector and act as the STMW-AAIW and AAIW-CDW interfaces.

Jointly, the two high-PV sheets in the Pacific and Indian basins, at the upper and lower boundaries of AAIW, give rise to the stratification maximum that defines the permanent pycnocline. In the Atlantic basin, the permanent pycnocline integrates only the denser high-PV sheet. (The lighter sheet is embedded within the subtropical gyre base, and thereby contributes to the ventilated pycnocline.) All in all, the pycnocline's structure documented here is found to correspond closely with that in hydrographic obser-

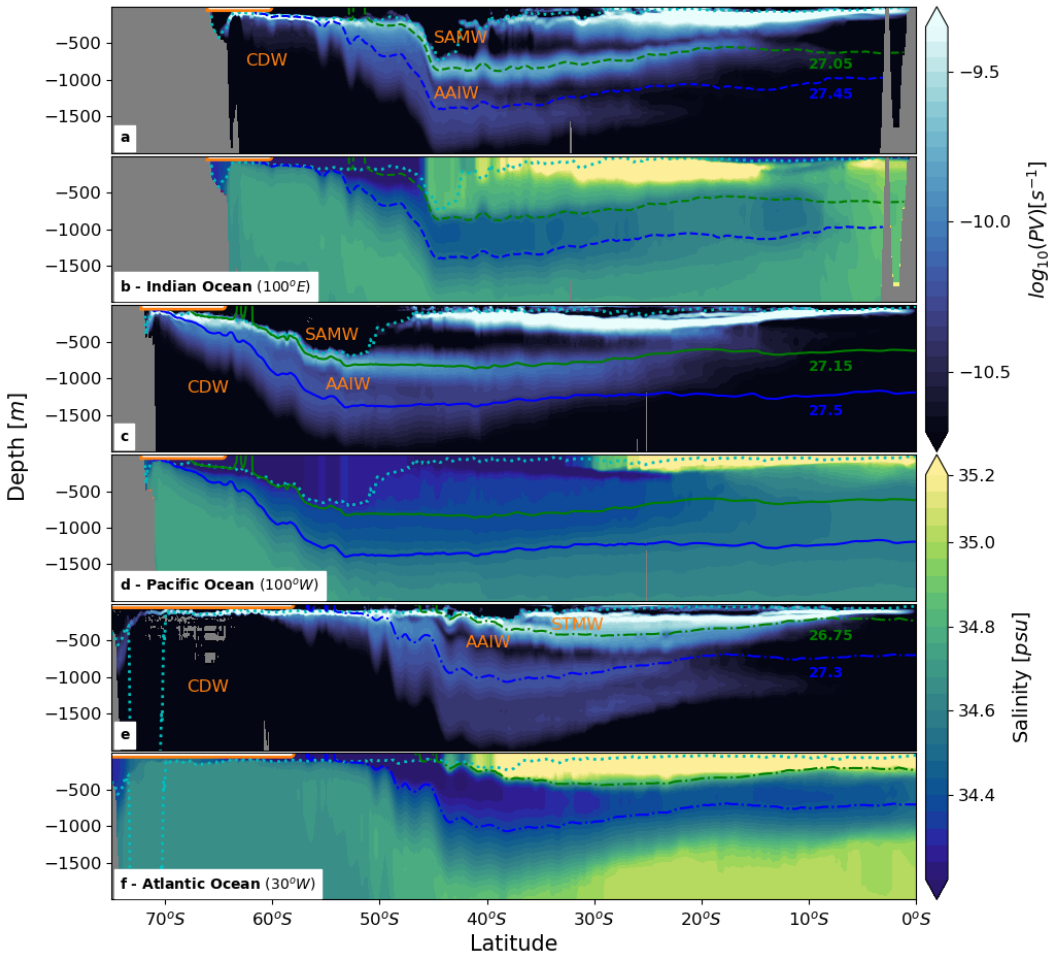

Figure 1. Potential vorticity and salinity. Winter values (shown for the month of September 2015) of (**a,c,e**) $log_{10}(|PV|)$ and (**b,d,f**) salinity for a representative section in (**a,b**) the South Indian Ocean (100^oE), (**c,d**) the South Pacific Ocean (100^oW) and (**e,f**) the South Atlantic Ocean (30^oW). Colored lines are isopycnal surfaces associated with the upper (green) and lower (blue) high-PV sheets. Subantarctic Mode Water (SAMW), Antarctic Intermediate Water (AAIW) and Circumpolar Deep Water (CDW) are labelled. The dashed cyan line represents the mixed layer depth. The orange line at the surface shows the sea ice extent, defined by sea ice concentrations in excess of 15%.

vations (Fig. A1; Appendix A), albeit these display a more subtle inter-sheet separation concealed by finescale processes (such as internal waves) absent from the model, and slight differences in the density of the high-PV sheets.

The anatomy of the high-PV sheets forming the permanent pycnocline offers several important hints as to the pycnocline's origin (Fig. 1 a,c,e). As one traces the high-PV sheets southward, approximately following isopycnals, their PV increases as the sheets draw near the surface in the seasonally ice-covered Southern Ocean. There, the high-PV sheets deviate significantly from density surfaces, as would be expected if diabatic or frictional processes were modifying PV locally. Thus, the structure of the high-PV sheets making up the Southern Hemisphere's permanent pycnocline suggests that the elevated stratification is generated in the upper layers of the seasonally ice-covered Southern Ocean. The generation mechanism of the high-PV sheets is assessed next.

3.2 High-PV generation in the ice-covered Southern Ocean

The generation of high PV in the ice-covered Southern Ocean may be understood in terms of two factors. First, the high-PV sheets originate near the surface in areas where salinity overwhelms temperature in determining stratification. This indicates that surface freshwater forcing is likely to play a central role in the creation of the high-PV sheets. Second, in order for these sheets to establish the permanent pycnocline, their stratification must survive PV destruction by surface buoyancy loss and vertical mixing in winter.

To further unravel these factors, the seasonal evolution of upper-ocean PV and salinity along a representative meridional section at 100°W, in the Pacific basin, is shown in Figure 2. Panels in each column correspond to every third month of the year, starting in December. Colored contours denote density surfaces of particular significance to the pycnocline's structure, as highlighted in Figure 1. The dashed cyan line marks the mixed layer base. The bottom panels provide the equivalent sections of potential temperature (Fig. 2 i) and the Stratification Control Index (SCI, Appendix B; (Fig. 2 j) in winter (shown for the month of September).

The highest PV values occur at the base of the buoyant mixed layer at the end of summer (Fig. 2 c), when inputs of ice melt, meteoric freshwater and heat create fresh and light Antarctic Surface Water (Fig. 2 d). The summer mixed layer base marks the loca-

tion of the seasonal pycnocline (Carmack, 2007; Pellichero et al., 2017). As the atmosphere cools and sea ice (shown by orange bars) rapidly expands in autumn, heat loss and brine rejection deepen the mixed layer and progressively erode the seasonal pycnocline (Fig. 2 e,f). The upper-ocean density increase and mixed layer deepening continue over winter (Fig. 2 g,h). Yet, despite the strong surface buoyancy loss and vertical mixing in autumn and winter, two distinct regions withstand the destruction of high PV at the base of the mixed layer. The 69-72°S latitude band holds the key to the generation and preservation of high PV along the 27.5 kg m^{-3} isopycnal (i.e. the denser of the permanent pycnocline's high-PV sheets), which reaches its shallowest point and highest PV there. The 63-69°S latitude band hosts the formation of the lighter (27.15 kg m^{-3}) of the high-PV sheets, which attains its maximum PV in the area. Both of these high-PV source regions are characterized by a SCI < -1 (Fig. 2 j): cold near-surface waters overlie warmer deeper waters in winter, and salinity determines upper-ocean stratification (Fig. 2 i).

The preferential imprinting of high PV on shallow isopycnals in the two highlighted regions begs the question of what sets these areas apart from the rest of the Southern Ocean. A first step toward an answer is provided by examination of the sea ice-ocean freshwater flux (Fig. 3 e; the total surface freshwater flux, including surface restoring terms, is shown in Fig. C1 and discussed in Appendix C). Both high-PV generation regions host net sea ice melt in winter. This counter-intuitive result has a different physical explanation in the southern and northern regions. In the southern area (69-72°S), net sea ice melt is related to upwelling of warm CDW (Wilson et al., 2019), which is shallowest in this region (Fig. 2 i). Once the seasonal pycnocline has been eliminated in the autumn, sea ice formation leads to entrainment of warm CDW into the surface mixed layer. The entrained heat melts the existing sea ice and hinders further ice formation. This well-documented negative feedback on sea ice formation (Martinson, 1990; Wilson et al., 2019) maintains the low salinity of the mixed layer. As a result, the strong, salinity-determined stratification (i.e. high PV) at the mixed layer base is preserved through winter (Fig. 2 g,j) against the upwelling of CDW (Evans et al., 2018). Thus, the isopycnal lying at the mixed layer base in the area (27.5 kg m^{-3}) is imprinted with high PV, despite never outcropping to the surface.

In contrast, north of 69°S in Figure 2, the sub-surface heat reservoir of CDW lies considerably deeper (Fig. 2 i) and no longer provides a leading-order feedback on the win-

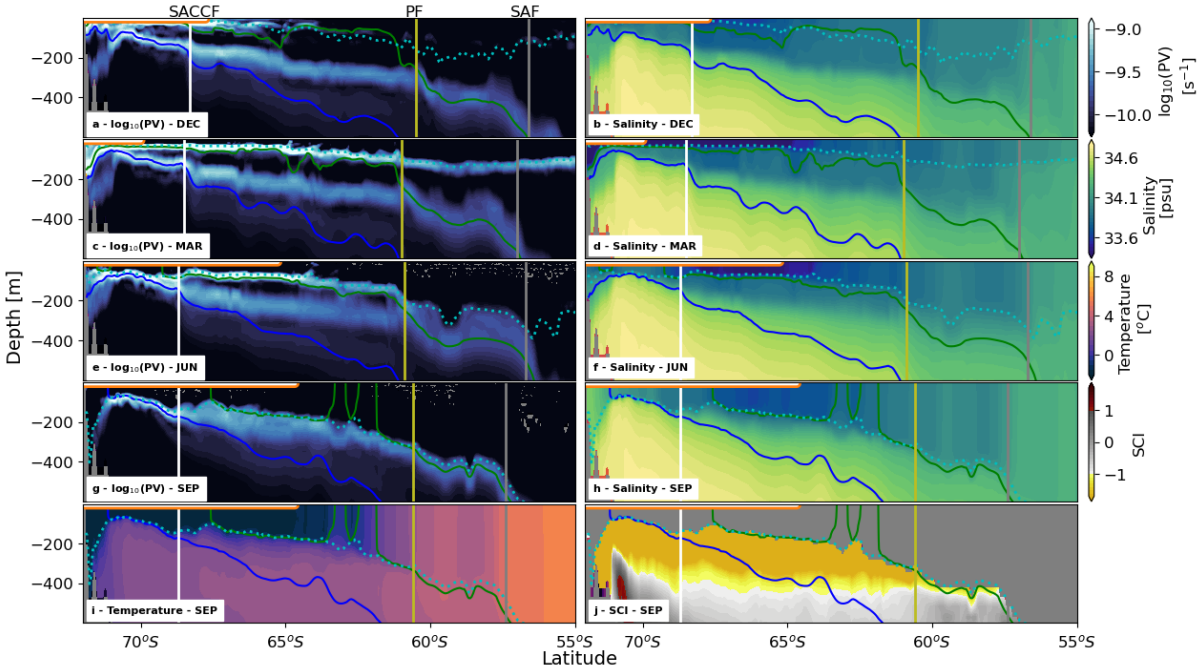

Figure 2. Seasonal evolution of potential vorticity and salinity in the Pacific sector. A latitude-depth section at 100°W of (**a,c,e,g**) $log_{10}(|PV|)$ and (**b,d,f,h**) salinity for (**a,b**) December, (**c,d**) March, (**e,f**) June, and (**g,h**) September of year 2014/2015. (**i**) Temperature, and (**j**) Stratification Control Index SCI at 100°W for June 2015. Colored lines are isopycnal surfaces $\sigma_\Theta = 27.15$ kg m^{-3} (green) and 27.5 kg m^{-3} (blue). Dashed cyan line shows the mixed-layer depth. Vertical lines mark Southern Ocean fronts, in particular, the Southern ACC front (SACCF; white), the Polar Front (PF; olive), and the Subantarctic Front (SAF; grey). Orange line at the surface shows the sea-ice extent, defined by sea-ice concentrations in excess of 15%.

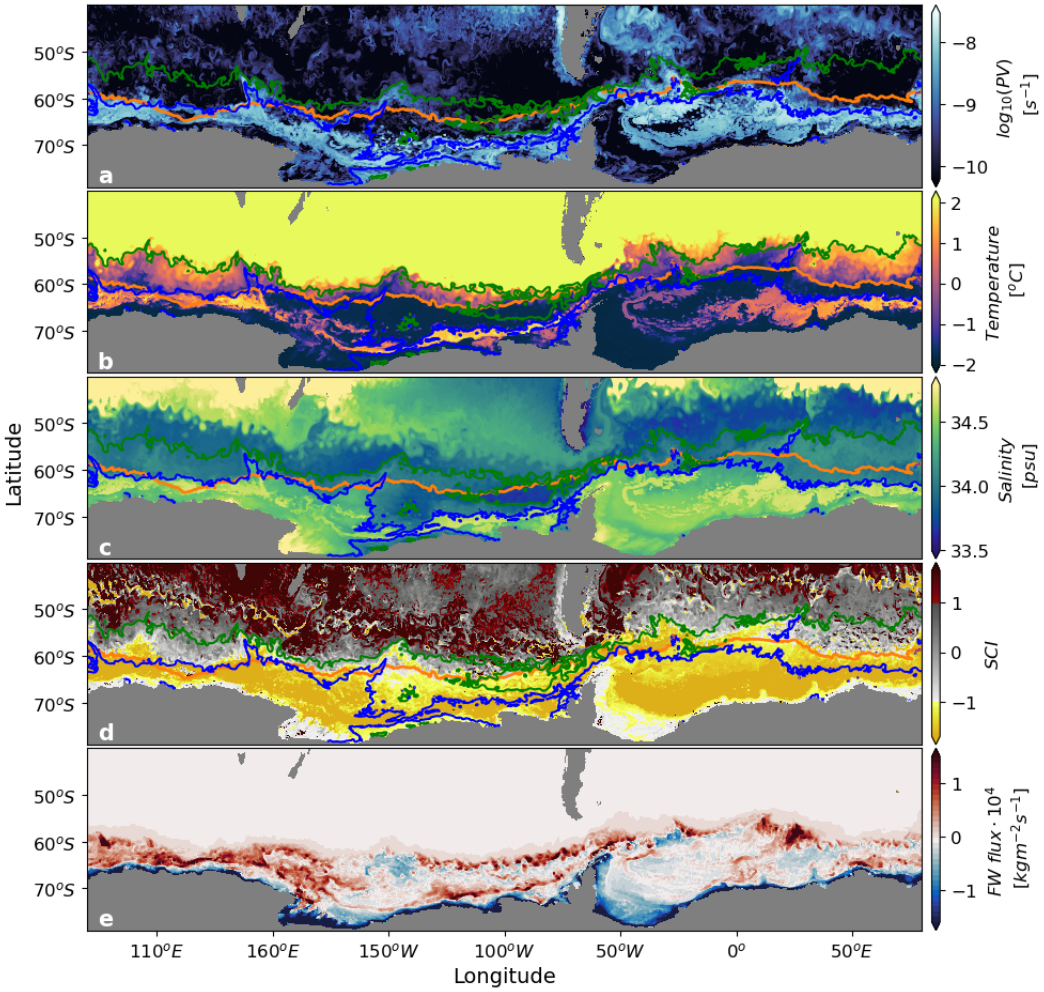

Figure 3. Circumpolar view of pycnocline formation in the upper ocean. (**a**) $log_{10}(|PV|)$, (**b**) temperature, (**c**) salinity, and (**d**) Stratification Control Index *SCI*, at a depth of 89 m in September 2015. (**e**) Wintertime (July to September 2015) mean of surface freshwater flux due to sea ice melting and freezing. Positive fluxes are directed into the ocean (melting ice). Green and blue contours respectively indicate isopycnal surfaces $\sigma_\Theta = 27.15$ kg m^{-3} and $\sigma_\Theta = 27.5$ kg m^{-3}. The orange line at the surface shows the sea ice extent, defined as the northern terminus of sea ice concentrations in excess of 15%.

tertime evolution of sea ice (Wilson et al., 2019). In this area, high-PV values below the mixed layer are maintained by the continuous influx of sea ice, which drifts from the main freezing sites near the Antarctic margins toward the open ocean (Haumann et al., 2016). The import of sea ice impedes wintertime PV destruction through two effects. First, the sea ice cover acts as a thermodynamic and mechanical insulator that dampens oceanic heat loss and wind-driven mechanical mixing (Sturm & Massom, 2009; Thorndike & Colony, 1982), and thus suppresses the erosion of upper-ocean stratification. Second, near and to the north of the winter sea ice edge, near-surface waters remain sufficiently warm year-round to melt sea ice drifting into the region (Fig. 3 b). Because of these two factors, sea ice melting prevails over much of the open Southern Ocean – including in winter (Fig. 3 e) – and the seasonal densification of the mixed layer is limited (Fig. 2 d-h). Hence, like in the southern high-PV source region, the surface mixed layer in this area remains very fresh in winter (Fig. 2 h), despite forcing by the cold and windy atmosphere and by diffusive salt gain from the underlying CDW. Elevated, salinity-determined stratification is then maintained year-round on the isopycnal lying at the base of the winter mixed layer (27.15 kg m^{-3}) in the area straddling the late winter sea ice edge, and the permanent pycnocline's lighter high-PV sheet is formed.

To the north of their formation sites, the two high-PV sheets are projected into the ocean interior along isopycnals at distinct locations (Fig. 2). These locations correspond with specific fronts of the Antarctic Circumpolar Current (ACC), where (sub-)mesoscale processes linked to the fronts' enhanced horizontal density gradients and vertical shears have been shown to induce along-isopycnal subduction of near-surface waters (A. Naveira Garabato et al., 2001; Klocker, 2018; Bachman & Klocker, 2020). Examination of Figure 2 indicates that the deeper of the high-PV sheets, extending along the 27.5 kg m^{-3} isopycnal in the Pacific basin, departs from the winter mixed layer base and dives into the interior at the Southern ACC Front (SACCF). Similarly, the shallower of the high-PV sheets, found at the 27.15 kg m^{-3} isopycnal in the Pacific sector, descends into the interior at the Polar Front (PF). These qualitative relationships between the spatial configuration of high-PV sheets and the ACC's frontal structure are reproduced all around the Southern Ocean (Figs. 2,4 and 5), and point to the existence of a dynamical underpinning of the sheets' downward and northward projection from their generation areas. While the precise nature of these dynamics cannot be ascertained with the model data available, we hypothesize that the high-PV sheets' descent into the interior is controlled

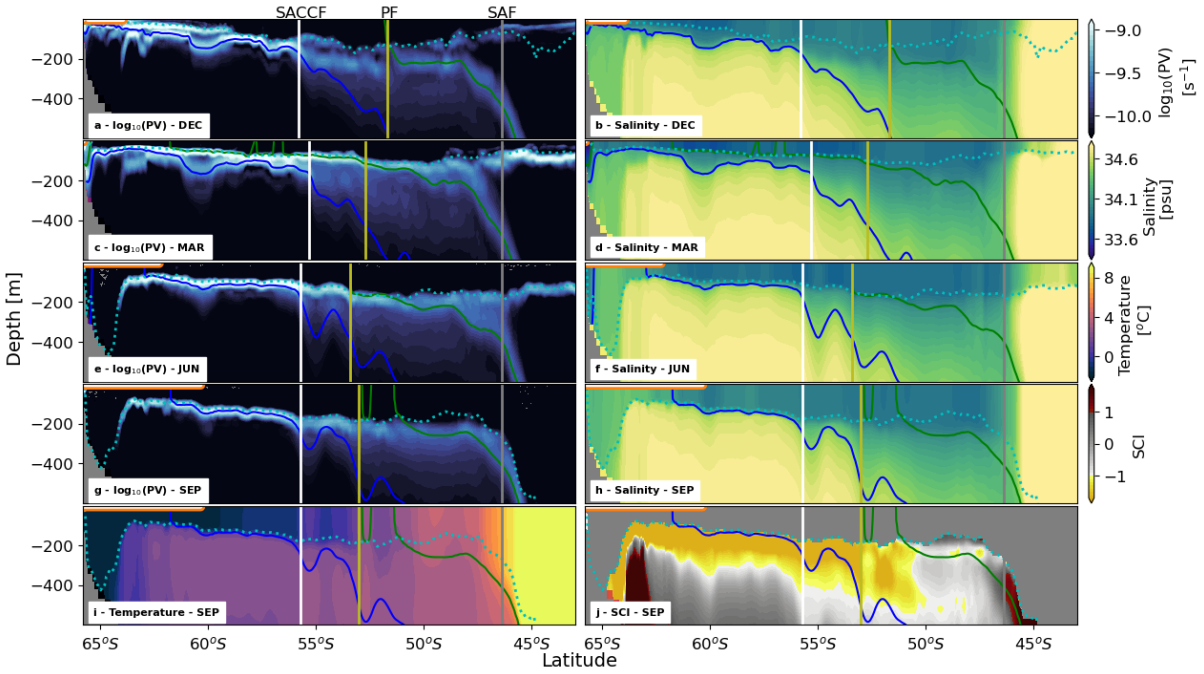

Figure 4. Seasonal evolution of potential vorticity and salinity in the Indian sector. A latitude-depth section at 100^{o}E of (**a,c,e,g**) $log_{10}(|PV|)$ and (**b,d,f,h**) salinity for (**a,b**) December, (**c,d**) March, (**e,f**) June, and (**g,h**) September of year 2014/2015. (**i**) Temperature, and (**j**) SCI at 100^{o}E for September 2015. Colored dashed lines are isopycnal surfaces σ_Θ = 27.05 kg m^{-3} (green) and 27.5 kg m^{-3} (blue). Dashed cyan line shows the mixed layer depth. Vertical lines mark Southern Ocean fronts, in particular the Southern ACC front (SACCF; white), the Polar Front (PF; olive), and the Subantarctic Front (SAF; grey). Orange line at the surface indicates the sea ice extent, defined by sea-ice concentrations in excess of 15%.

by the same processes that govern frontal subduction (A. Naveira Garabato et al., 2001). Establishing whether this control is exerted directly via the northward transport of elevated PV along the pycnocline's isopycnals, or indirectly via the absence of low-PV injection on those isopycnals, will be the subject of a follow-up study.

3.3 Circumpolar view of Southern Ocean permanent pycnocline generation

The permanent pycnocline-generating processes identified above with a meridional section in the Pacific basin (Fig. 2) are widely generic around the Southern Ocean. To elicit this point, Figures 3 a-d compare the horizontal distributions of wintertime (shown

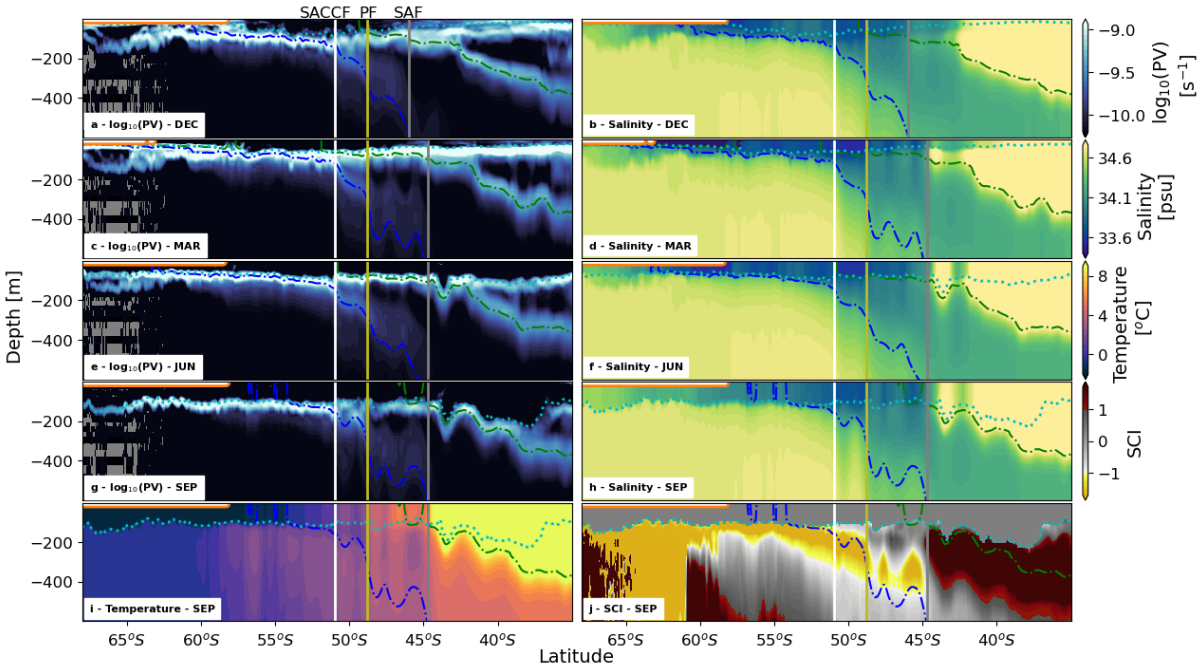

Figure 5. Seasonal evolution of potential vorticity and salinity in the Atlantic sector. A latitude-depth section at 30^{o}W of (**a,c,e,g**) $log_{10}(|PV|)$ and (**b,d,f,h**) salinity for (**a,b**) December, (**c,d**) March, (**e,f**) June, and (**g,h**) September of year 2014/2015. (**i**) Temperature, and (**j**) SCI at 30^{o}W for September 2015. Colored dash-dotted lines are isopycnal surfaces σ_Θ = 27.15 kg m^{-3} (green) and 27.5 kg m^{-3} (blue). Dashed cyan line shows the mixed layer depth. Vertical lines mark Southern Ocean fronts, in particular the Southern ACC front (SACCF; white), the Polar Front (PF; olive), and the Subantarctic Front (SAF; grey). Orange line at the surface indicates the sea-ice extent, defined by sea ice concentrations in excess of 15%.

for the month of September) upper-ocean PV, thermohaline properties and SCI at an illustrative depth of 89 m, which is close to the base of the winter mixed layer south of the PF (Fig. 2). The wintertime surface freshwater flux due to the melting and freezing of sea ice is also shown in Figure 3 e.

Wintertime upper-ocean PV is elevated along a several hundred kilometre-wide, circumpolar swath immediately to the north of the Antarctic continental shelf break (light blue shading in Fig. 3 a). This swath delineates the generation area of the denser high-PV sheet, as can be gleaned from the approximate spatial correspondence between the band of increased PV and the 27.5 kg m^{-3} isopycnal (blue contour in Fig. 3 a), on which that high-PV sheet lies in the Pacific basin. The lighter high-PV sheet, formed further to the north, is not visible in this map because its generation takes place at a greater depth (see the high-PV sheet on the green isopycnal in Fig. 2 g). The swath of elevated PV encircling Antarctica coincides with an area of higher temperature (Fig. 3 b) and salinity (Fig. 3 c), and reduced SCI (SCI < -1, yellow shading in Fig. 3 d). These indicate the shoaling of relatively warm and saline CDW beneath cold and fresh near-surface waters, which gives rise to strong, salinity-determined upper-ocean stratification. The association of high-PV generation, CDW shoaling and elevated salinity-induced stratification with the ice-ocean feedback outlined above (Martinson, 1990; Wilson et al., 2019) is supported by the horizontal distribution of the surface freshwater flux due to the melting and freezing of sea ice (Fig. 3 e): the swath of high PV is broadly aligned with a band of substantial freshwater input to the ocean (red shading) fringing the Antarctic continental shelf break.

A second region of enhanced surface freshwater input occurs further to the north, around the winter sea ice edge (Fig. 3 e), and is linked to the generation of the lighter high-PV sheet. The excess freshwater forcing in this area produces an abrupt northward reduction in mixed layer salinity (Fig. 3 c), and is associated with a meridional transition from near-freezing to above-zero mixed layer temperature (Fig. 3 b). Such thermohaline signatures suggest that the reduction in salinity stems at least in part from the melting of sea ice transported into warmer surface waters via wind-driven, northward Ekman drift (Haumann et al., 2016). More generally, persistent surface freshwater gain in this circumpolar band of reduced surface salinity enables the preservation of elevated PV at the winter mixed layer base on the isopycnal coincident with the lighter high-PV sheet.

Although the key pycnocline formation features highlighted above are quasi-circumpolar, some differences between distinct sectors of the Southern Ocean are also apparent (cf. Figs. 2, 4 and 5). Most notably, the South Atlantic permanent pycnocline incorporates one high-PV sheet only, at a considerably lighter isopycnal than the denser high-PV sheets in the Indo-Pacific sector. This is because, upon entering the South Atlantic, the ACC veers sharply northward, leading to a significant rearrangement of ACC frontal locations and surface buoyancy flux patterns. As a result, unlike in the other basins, the SACCF in the South Atlantic lies consistently to the north of the winter sea ice edge, such that all melt-generated, high-PV waters at the winter mixed layer base within this sector are collated into a single sheet descending into the interior at the SACCF (Fig. S3). The additional, shallower and lighter high-PV sheet formed in the Atlantic basin (see section 3.1) contributes to the ventilated pycnocline, and qualitatively conforms to the internal boundary layer of classical pycnocline theories.

4 Conclusions and Outlook

The main result of this work is that the generation of the defining feature of the permanent pycnocline in the Southern Ocean and neighbouring Southern Hemisphere basins – elevated mid-depth stratification – is governed by forcings and processes that are distinct from those highlighted by classical views of pycnocline formation (Welander, 1959; Luyten et al., 1983; Huang, 1988; Robinson & Stommel, 1959; Stommel & Webster, 1962; Young & Ierley, 1986; Salmon, 1990) in four significant ways.

First, the Southern Ocean permanent pycnocline's high stratification is primarily sourced under the seasonal sea ice (Fig. 1), where stratification is determined by salinity (the beta ocean), rather than widely across regions of the subtropical and subpolar oceans with temperature-determined stratification (the alpha ocean), as suggested by classical theories. It remains to be established how the processes highlighted by such theories interact with the mechanism put forward in this work to determine the permanent pycnocline's structure across alpha and beta oceans. This will be investigated in follow-up work.

Second, the key external forcing driving the formation of the Southern Ocean permanent pycnocline's enhanced stratification is not atmospheric cooling, as broadly proposed in classical views (Wolfe & Cessi, 2010; Nikurashin & Vallis, 2012), but freshwa-

ter input by sea ice melt in winter. The melting is focused in two distinct zones: one offshore of the Antarctic continental shelf break, where sea ice melt is sustained by the upward entrainment of warm CDW (Martinson, 1990; Wilson et al., 2019), and another fringing the winter sea ice edge, where sea ice melts as it drifts northward into warmer surface waters (Haumann et al., 2016). These two wintertime melting zones give rise to two sheets of high stratification, and confer the pycnocline with a double stratification-maximum structure (Fig. 1). This highlights how the strong coupling between thermal and freshwater forcings associated with sea ice formation and melt acts to configure ocean stratification on basin scales.

Third, the production of high stratification within the Southern Ocean permanent pycnocline does not stem from the downward projection of a meridional surface density gradient along outcropping isopycnals, as in classical theories (Luyten et al., 1983; Samelson & Vallis, 1997), but rather from the production of a vertical density gradient at the base of the winter mixed layer. Thus, the density classes hosting the permanent pycnocline across and beyond the Southern Ocean need not reach the surface to acquire their elevated stratification. This implies that the permanent pycnocline's density structure may be controlled by sub-surface mixing processes around the mixed layer base, rather than directly by buoyancy fluxes across the ocean surface.

Fourth, our finding that the descent of the permanent pycnocline's high-stratification sheets into the ocean interior is localized to specific ACC fronts suggests that (sub-)mesoscale upper-ocean frontal dynamics may shape this stage of pycnocline formation. This contrasts with classical views, which rationalize the downward projection of the pycnocline in terms of large-scale, wind-driven Ekman flows and, in some cases, the integrated effects of deep baroclinic eddies (Wolfe & Cessi, 2010; Nikurashin & Vallis, 2012).

In conclusion, the elevated stratification that defines the Southern Ocean permanent pycnocline is generated by seasonal sea ice-ocean interactions, and may be projected equatorward by upper-ocean frontal processes. Both of these elements are absent from current theoretical perspectives on pycnocline formation, including those considering the Southern Ocean's role (Gnanadesikan, 1999; Wolfe & Cessi, 2010; Nikurashin & Vallis, 2012; D. P. Marshall et al., 2017). Such Southern Ocean-focused theories reveal the permanent pycnocline's depth to be determined by an intricate interplay between wind forcing, baroclinic eddies and surface buoyancy fluxes. However, they assume that the per-

manent pycnocline's stratification reflects the meridional density gradient at the surface of the Southern Ocean, and that this gradient is set by annual-mean surface heat fluxes. Our work indicates that establishment of the permanent pycnocline depends on the coupled seasonal evolution of sea ice-induced freshwater forcing, upper-ocean density structure, and sub-surface mixing processes.

Appendix A Model comparison with observations

While the model is thoroughly validated elsewhere (Kiss et al., 2020), for the purpose of this work we note that the model adequately reproduces the observed structure of the permanent pycnocline (cf. Figs. 1 and A1), with two modest differences. First, the separation between high-stratification sheets in the observations is more subtle than in the model. This is due at least in part to contamination of the observational picture by finescale motions (e.g., internal waves) and measurement noise. It is also likely that the model exaggerates the inter-sheet gap in the ocean interior, as the model's limited resolution does not fully capture the (sub-)mesoscale re-stratification processes expected to moderate vertical gradients in interior stratification (Bachman & Klocker, 2020). Second, the densities of the observed high-stratification sheets are slightly lighter (typically by 0.1 - 0.2 kg m^{-3}) than those in the model.

Appendix B Stratification Control Index

A key theoretical concept in our analysis of the model simulation is the Stratification Control Index, SCI, which is considered here to assess the degree of spiciness in a stable stratification (Stewart & Haine, 2016). The SCI is defined as the ratio of the spice frequency, $K^2 = g(\alpha\partial_z\Theta + \beta\partial_z S_A)$, to the buoyancy frequency, $N^2 = g(\alpha\partial_z\Theta - \beta\partial_z S_A)$, where g is the gravitational acceleration, α is the thermal expansion coefficient, and β is the haline contraction coefficient (Ioc et al., 2010). Since planetary PV is proportional to the stratification, SCI can equally be interpreted to indicate the relative contributions of temperature and salinity to setting PV. By construction, the SCI has three distinct regimes: SCI < -1 corresponds to a stable stratification controlled by salinity where the thermal stratification is unstable (as often found in polar regions); $-1 <$ SCI < 1 is associated with thermal and haline stratifications that are both stable; and SCI > 1 is obtained when temperature controls the density stratification in the presence of a destabilizing effect of salinity.

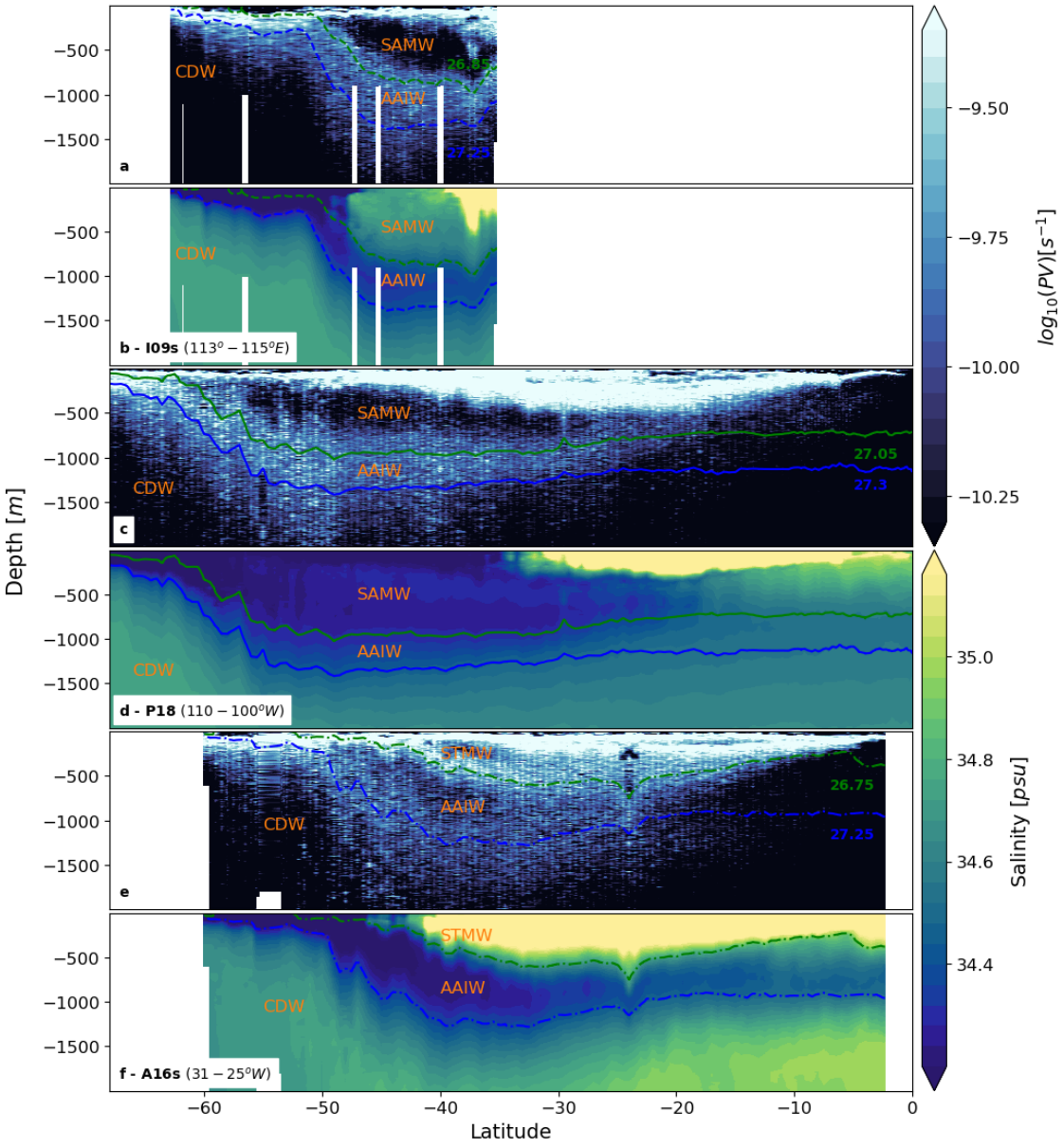

Figure A1. Potential vorticity and salinity from observations. Ship-based observations of (**a,c,e**) $log_{10}(|PV|)$ and (**b,d,f**) salinity. (**a,b**) WOCE transect I09s from a R/V Aurora Australis cruise in January-February 2012, (**c,d**) WOCE transect P18 from a R/V Ronald H. Brown cruise in November 2016 - February 2017, and (**e,f**) WOCE transect A16s from R/V Ronald H. Brown cruise in January-February 2005. Colored lines are isopycnal surfaces approximately associated with the upper (green) and lower (blue) high-PV sheets. Subtropical Mode Water (STMW), Subantarctic Mode Water (SAMW), Antarctic Intermediate Water (AAIW), and Circumpolar Deep Water (CDW) are labeled.

The SCI can be connected to several other stratification indicators more commonly used in the literature. The density ratio, $R_\sigma = (\alpha\partial_z\Theta)/(\beta\partial_z S_A)$, was first introduced by Turner (Turner, 1973) and can be related to the SCI as $R_\sigma = (\mathrm{SCI}+1)(\mathrm{SCI}-1)$. A difficulty with the density ratio is that it diverges when the salinity stratification vanishes, even in the presence of a stable thermal stratification. This is the reason why the SCI is preferred here. Subsequently, the Turner angle was also determined as the arc tangent of the ratio of spice to buoyancy frequencies (Ruddick, 1983). Hence, the SCI is simply the tangent of the Turner angle, uniquely defined for any stable stratification. Drawing on the properties of the Turner angle, salt fingering is implied to occur when $\mathrm{SCI} > 1$, and diffusive convection develops when $\mathrm{SCI} < -1$.

Appendix C Thermal and haline surface buoyancy fluxes

The surface buoyancy flux, B, depends on both surface heating and freshwater input, and can be expressed as (Cronin & Sprintall, 2001)

$$B = \underbrace{-\frac{g\alpha Q}{\rho c_p}}_{B_H} + \underbrace{g\beta F_w SSS}_{B_{FW}}, \tag{C1}$$

where B_H is the buoyancy flux due to heating and cooling, and B_{FW} is the buoyancy flux due to freshwater input or loss. Q is the surface heat flux, F_w the surface freshwater input, ρ the surface density, c_p the specific heat capacity of seawater, and SSS the sea surface salinity. Q has units of W m^{-2}, F_w has units of m s^{-1}, and B has units of m^2 s^{-3}. In the coupled sea ice-ocean model used here, surface fluxes are due to (i) restoring to temperature and salinity at the sea surface in the JRA55-do v1.3 forcing data set, and (ii) freshwater fluxes resulting from the melting and freezing of sea ice. In winter (Fig. C1, showing a mean over July-September 2015), the surface buoyancy flux indicates that changes in upper-ocean buoyancy under sea ice are almost entirely due to freshwater fluxes induced by the melting and freezing of sea ice. North of the sea ice edge, the surface buoyancy flux transitions to being largely dominated by surface heat fluxes.

Acknowledgments

The authors thank the Consortium for Ocean-Sea Ice Modeling in Australia (COSIMA; www.cosima.org.au) for making the ACCESS-OM2 suite of models available at github.com/COSIMA/access-om2. Model runs were undertaken with the assistance of resources from the National Computational Infrastructure (NCI), which is supported by

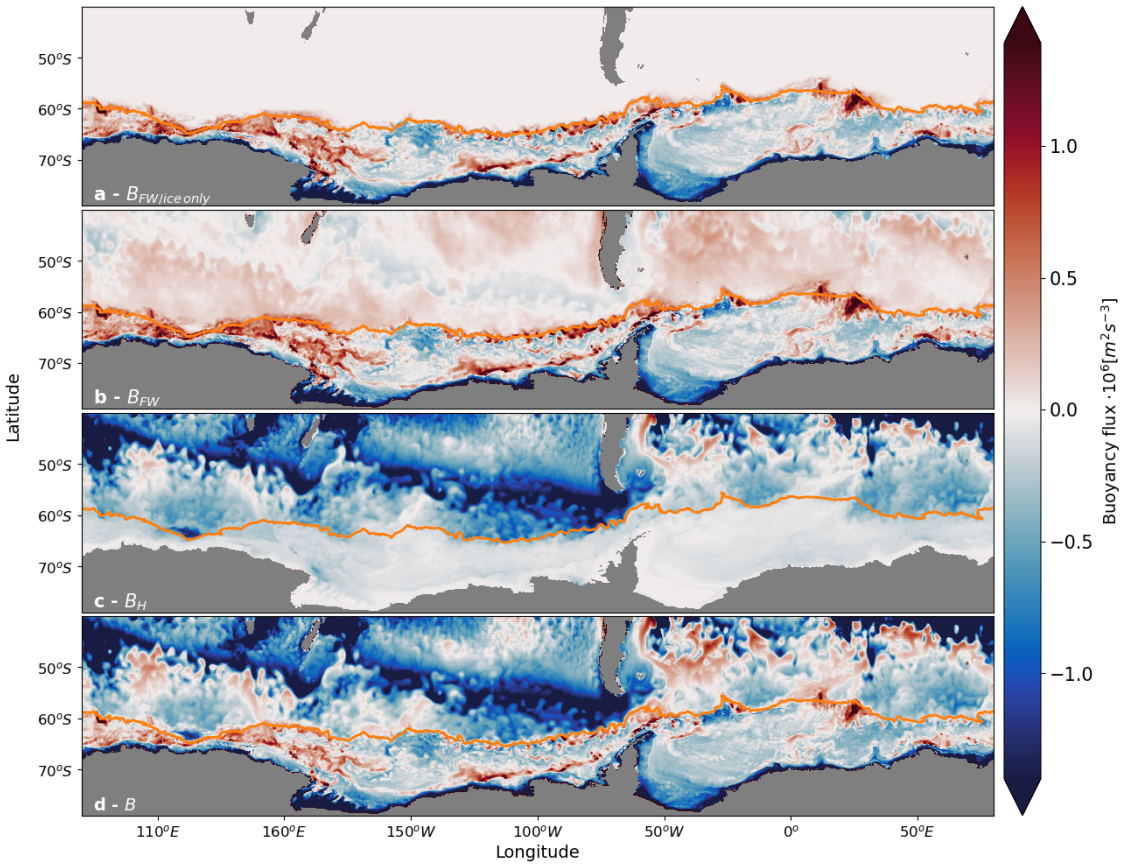

Figure C1. Surface buoyancy flux in the Southern Ocean. Wintertime (mean over July-September 2015) surface buoyancy flux due to (**a**) freshwater from sea ice melting and freezing, (**b**) total surface freshwater input, and (**c**) surface heat flux. (**d**) Net surface buoyancy flux. Positive fluxes are directed into the ocean. The orange line shows the sea-ice extent, defined as the northern terminus of sea ice concentrations in excess of 15%.

the Australian Government. This research was supported under Australian Research Council's Special Research Initiative for Antarctic Gateway Partnership (Project ID SR140300001). This project received grant funding from the Australian Government as part of the Antarctic Science Collaboration Initiative program. The work was supported in part by the Centre for Southern Hemisphere Oceans Research, a partnership between CSIRO, the Qingdao National Laboratory for Marine Science and Technology, the University of New South Wales and the University of Tasmania and by the Australian Antarctic Program Partnership. All the data used in this work are publicly available. The model code is available at
github.com/COSIMA/access-om2, and the model output can be accessed at
http://dx.doi.org/10.4225/41/5a2dc8543105a. Observational transects can be downloaded at https://cchdo.ucsd.edu/cruise/09AR20120105 (WOCEtransect I09s),
https://cchdo.ucsd.edu/cruise/33RO20161119 (WOCE transect P18), and
https://cchdo.ucsd.edu/cruise/33RO200501 (WOCE transect A16s).

References

Bachman, S., & Klocker, A. (2020). Interaction of jets and submesoscale dynamics leads to rapid ocean ventilation. *J. Phys. Oceanogr.*, *50*(10). doi: 10.1175/JPO-D-20-0117.1

Bullister, J. L., Rhein, M., & Mauritzen, C. (2001). Deepwater Formation. In G. Siedler, S. M. Griffies, J. Gould, & J. A. Church (Eds.), *Ocean circ. clim. a 21st century perspect.* (pp. 227–253). Academic Press.

Carmack, E. C. (2007). The alpha/beta ocean distinction: A perspective on freshwater fluxes, convection, nutrients and productivity in high-latitude seas. *Deep. Res. Part II Top. Stud. Oceanogr.*, *54*(23-26), 2578–2598. doi: 10.1016/j.dsr2.2007.08.018

Cronin, M., & Sprintall, J. (2001). Wind And Buoyancy-forced Upper Ocean. In *Encycl. ocean sci.* (pp. 3219–3226). Elsevier. doi: 10.1006/rwos.2001.0157

DeVries, T., & Primeau, F. (2011). Dynamically and observationally constrained estimates of water-mass distributions and ages in the global ocean. *J. Phys. Oceanogr.*, *41*(12), 2381–2401. doi: 10.1175/JPO-D-10-05011.1

DeVries, T., & Weber, T. (2017). The export and fate of organic matter in the ocean: New constraints from combining satellite and oceanographic

tracer observations. *Global Biogeochem. Cycles*, *31*(3), 535–555. doi: 10.1002/2016GB005551

Evans, D. G., Zika, J. D., Naveira Garabato, A. C., & Nurser, A. J. (2018). The Cold Transit of Southern Ocean Upwelling. *Geophys. Res. Lett.*, *45*(24), 13,386–13,395. doi: 10.1029/2018GL079986

Gnanadesikan, A. (1999, mar). A Simple Predictive Model for the Structure of the Oceanic Pycnocline. *Science (80-.).*, *283*(5410), 2077–2079. doi: 10.1126/science.283.5410.2077

Haumann, F. A., Gruber, N., Münnich, M., Frenger, I., & Kern, S. (2016). Sea-ice transport driving Southern Ocean salinity and its recent trends. *Nature*, *537*(7618), 89–92. doi: 10.1038/nature19101

Huang, R. X. (1988, apr). On Boundary Value Problems of the Ideal-Fluid Thermocline. *J. Phys. Oceanogr.*, *18*(4), 619–641. doi: 10.1175/1520-0485(1988)018⟨0619:OBVPOT⟩2.0.CO;2

Ioc, Scor, & Iapso. (2010). The international thermodynamic equation of seawater – 2010: Calculation and use of thermodynamic properties. *Intergov. Oceanogr. Comm. Manuals Guid. No. 56*(June), 196.

Kiss, A., McC Hogg, A., Hannah, N., Boeira Dias, F., B Brassington, G., Chamberlain, M., ... Zhang, X. (2020). ACCESS-OM2 v1.0: A global ocean-sea ice model at three resolutions. *Geosci. Model Dev.*, *13*(2). doi: 10.5194/gmd-13-401-2020

Klocker, A. (2018). Opening the window to the Southern Ocean: The role of jet dynamics. *Sci. Adv.*, *4*(10). doi: 10.1126/sciadv.aao4719

Lecomte, O., Goosse, H., Fichefet, T., De Lavergne, C., Barthélemy, A., & Zunz, V. (2017). Vertical ocean heat redistribution sustaining sea-ice concentration trends in the Ross Sea. *Nat. Commun.*, *8*(1). doi: 10.1038/s41467-017-00347-4

Luyten, J. R., Pedlosky, J., & Stommel, H. (1983, feb). The Ventilated Thermocline. *J. Phys. Oceanogr.*, *13*(2), 292–309. doi: 10.1175/1520-0485(1983)013⟨0292:TVT⟩2.0.CO;2

Marshall, D. P., Ambaum, M. H., Maddison, J. R., Munday, D. R., & Novak, L. (2017). Eddy saturation and frictional control of the Antarctic Circumpolar Current. *Geophys. Res. Lett.*, *44*(1), 286–292. doi: 10.1002/2016GL071702

Marshall, J., Olbers, D., Ross, H., & Wolf-Gladrow, D. (1993, mar). Potential Vorticity Constraints on the Dynamics and Hydrography of the Southern Ocean. *J. Phys. Oceanogr.*, *23*(3), 465–487. doi: 10.1175/1520-0485(1993)023⟨0465:PVCOTD⟩2.0.CO;2

Martinson, D. G. (1990). Evolution of the southern ocean winter mixed layer and sea ice: Open ocean deepwater formation and ventilation. *J. Geophys. Res.*, *95*(C7), 11641. doi: 10.1029/jc095ic07p11641

McCartney, M. S. (1977). Subantarctic Mode Water. *Deep. Res.*, *24*, 103–119.

Naveira Garabato, A., Allen, J., Leach, H., Strass, V., Pollard, R., Garabato, A., & Leach, H. (2001). Mesoscale subduction at the Antarctic Polar Front driven by baroclinic instability. *J. Phys. Oceanogr.*, 2087–2107. doi: 10.1175/1520-0485(2001)031⟨2087:MSATAP⟩2.0.CO;2

Naveira Garabato, A. C., Williams, A. P., & Bacon, S. (2014). The three-dimensional overturning circulation of the Southern Ocean during the WOCE era. *Prog. Oceanogr.*, *120*, 41–78. doi: 10.1016/j.pocean.2013.07.018

Nikurashin, M., & Vallis, G. (2012). A theory of the interhemispheric meridional overturning circulation and associated stratification. *J. Phys. Oceanogr.*, *42*(10), 1652–1667. doi: 10.1175/JPO-D-11-0189.1

Nycander, J., Hieronymus, M., & Roquet, F. (2015). The nonlinear equation of state of sea water and the global water mass distribution. *Geophys. Res. Lett.*, *42*(18), 7714–7721. doi: 10.1002/2015GL065525

Pellichero, V., Sallée, J.-B., Schmidtko, S., Roquet, F., & Charrassin, J.-B. (2017, feb). The ocean mixed layer under Southern Ocean sea-ice: Seasonal cycle and forcing. *J. Geophys. Res. Ocean.*, *122*(2), 1608–1633. doi: 10.1002/2016JC011970

Polyakov, I. V., Pnyushkov, A. V., Alkire, M. B., Ashik, I. M., Baumann, T. M., Carmack, E. C., ... Yulin, A. (2017). Greater role for Atlantic inflows on sea-ice loss in the Eurasian Basin of the Arctic Ocean. *Science (80-.).*, *356*(6335), 285–291. doi: 10.1126/science.aai8204

Robinson, A., & Stommel, H. (1959). The Oceanic Thermocline and the Associated Thermohaline Circulation. *Tellus*, *11*(3), 295–308. doi: 10.3402/tellusa.v11i3.9317

Roquet, F., Madec, G., Brodeau, L., & Nycander, J. (2015). Defining a simpli-

fied yet "Realistic" equation of state for seawater. *J. Phys. Oceanogr.*, *45*(10), 2564–2579. doi: 10.1175/JPO-D-15-0080.1

Ruddick, B. (1983). A practical indicator of the stability of the water column to double-diffusive activity. *Deep Sea Res. Part A, Oceanogr. Res. Pap.*, *30*(10), 1105–1107. doi: 10.1016/0198-0149(83)90063-8

Salmon, R. (1990, aug). The thermocline as an "internal boundary layer". *J. Mar. Res.*, *48*(3), 437–469. doi: 10.1357/002224090784984650

Samelson, R. M., & Vallis, G. K. (1997). Large-scale circulation with small diapycnal diffusion: The two-thermocline limit. *J. Mar. Res.*, *55*(2), 223–275. doi: 10.1357/0022240973224382

Speer, K., & Forget, G. (2001). Global Distribution and Formation of Mode Waters. In G. Siedler, S. M. Griffies, J. Gould, & J. A. Church (Eds.), *Ocean circ. clim. a 21st century perspect.* (pp. 211–226). Academic Press.

Stewart, K. D., & Haine, T. W. (2016). Thermobaricity in the transition zones between alpha and beta oceans. *J. Phys. Oceanogr.*, *46*(6), 1805–1821. doi: 10.1175/JPO-D-16-0017.1

Stommel, H., & Webster, J. (1962). Some properties of thermocline equations in a subtropical gyre. *J. Mar. Res.*, *20*(1), 42–56.

Sturm, M., & Massom, R. A. (2009). Snow and Sea Ice. In *Sea ice* (pp. 153–204). Oxford, UK: Wiley-Blackwell. doi: 10.1002/9781444317145.ch5

Talley, L. D. (2013). Closure of the global overturning circulation through the Indian, Pacific, and southern oceans. *Oceanography*, *26*(1), 80–97. doi: 10.5670/oceanog.2013.07

Tamsitt, V., Drake, H. F., Morrison, A. K., Talley, L. D., Dufour, C. O., Gray, A. R., ... Weijer, W. (2017). Spiraling pathways of global deep waters to the surface of the Southern Ocean. *Nat. Commun.*, *8*(1), 1–10. doi: 10.1038/s41467-017-00197-0

Thorndike, A. S., & Colony, R. (1982). Sea ice motion in response to geostrophic winds. *J. Geophys. Res.*, *87*(C8), 5845. doi: 10.1029/jc087ic08p05845

Turner, J. S. (1973). *Buoyancy Effects in Fluids.* Cambridge University Press. doi: 10.1017/CBO9780511608827

Vallis, G. K. (2000). Large-scale circulation and production of stratification: Effects of wind, geometry, and diffusion. *J. Phys. Oceanogr.*, *30*(5), 933–954. doi: 10

.1175/1520-0485(2000)030⟨0933:LSCAPO⟩2.0.CO;2

Welander, P. (1959, aug). An Advective Model of the Ocean Thermocline. *Tellus*, *11*(3), 309–318. doi: 10.3402/tellusa.v11i3.9316

Wilson, E. A., Riser, S. C., Campbell, E. C., & Wong, A. P. (2019). Winter upper-ocean stability and ice-ocean feedbacks in the sea ice-covered Southern Ocean. *J. Phys. Oceanogr.*, *49*(4), 1099–1117. doi: 10.1175/JPO-D-18-0184.1

Wolfe, C. L., & Cessi, P. (2010). What sets the strength of the middepth stratification and overturning circulation in eddying ocean models? *J. Phys. Oceanogr.*, *40*(7), 1520–1538. doi: 10.1175/2010JPO4393.1

Young, W. R., & Ierley, G. R. (1986, nov). Eastern Boundary Conditions and Weak Solutions of the Ideal Thermocline Equations. *J. Phys. Oceanogr.*, *16*(11), 1884–1900. doi: 10.1175/1520-0485(1986)016⟨1884:EBCAWS⟩2.0.CO;2